ACS APPLIED MATERIALS & INTERFACES

Research Article

www.acsami.org

Trimethylaluminum and Oxygen Atomic Layer Deposition on Hydroxyl-Free Cu(111)

Amir Gharachorlou,[†,⊥] Michael D. Detwiler,[†,⊥] Xiang-Kui Gu,[†] Lukas Mayr,[‡,§] Bernhard Klötzer,[‡] Jeffrey Greeley,[†] Ronald G. Reifenberger,[§,∥] W. Nicholas Delgass,[†] Fabio H. Ribeiro,[†] and Dmitry Y. Zemlyanov*[,§]

[†]School of Chemical Engineering, Purdue University, West Lafayette, Indiana 47907, United States

[‡]Institute for Physical Chemistry, University of Innsbruck, A-6020 Innsbruck, Austria

[§]Birck Nanotechnology Center, Purdue University, West Lafayette, Indiana 47907, United States

[∥]Department of Physics, Purdue University, West Lafayette, Indiana 47907, United States

Supporting Information

ABSTRACT: Atomic layer deposition (ALD) of alumina using trimethylaluminum (TMA) has technological importance in microelectronics. This process has demonstrated a high potential in applications of protective coatings on Cu surfaces for control of diffusion of Cu in Cu_2S films in photovoltaic devices and sintering of Cu-based nanoparticles in liquid phase hydrogenation reactions. With this motivation in mind, the reaction between TMA and oxygen was investigated on Cu(111) and Cu_2O/Cu(111) surfaces. TMA did not adsorb on the Cu(111) surface, a result consistent with density functional theory (DFT) calculations predicting that TMA adsorption and decomposition are thermodynamically unfavorable on pure Cu(111). On the other hand, TMA readily adsorbed on the Cu_2O/Cu(111) surface at 473 K resulting in the reduction of some surface Cu^{1+} to metallic copper (Cu^0) and the formation of a copper aluminate, most likely $CuAlO_2$. The reaction is limited by the amount of surface oxygen. After the first TMA half-cycle on Cu_2O/Cu(111), two-dimensional (2D) islands of the aluminate were observed on the surface by scanning tunneling microscopy (STM). According to DFT calculations, TMA decomposed completely on Cu_2O/Cu(111). High-resolution electron energy loss spectroscopy (HREELS) was used to distinguish between tetrahedrally (Al_{tet}) and octahedrally (Al_{oct}) coordinated Al^{3+} in surface adlayers. TMA dosing produced an aluminum oxide film, which contained more octahedrally coordinated Al^{3+} (Al_{tet}/Al_{oct} HREELS peak area ratio ≈ 0.3) than did dosing O_2 (Al_{tet}/Al_{oct} HREELS peak area ratio ≈ 0.5). After the first ALD cycle, TMA reacted with both Cu_2O and aluminum oxide surfaces in the absence of hydroxyl groups until film closure by the fourth ALD cycle. Then, TMA continued to react with surface Al−O, forming stoichiometric Al_2O_3. O_2 half-cycles at 623 K were more effective for carbon removal than O_2 half-cycles at 473 K or water half-cycles at 623 K. The growth rate was approximately 3−4 Å/cycle for TMA+O_2 ALD (O_2 half-cycles at 623 K). No preferential growth of Al_2O_3 on the steps of Cu(111) was observed. According to STM, Al_2O_3 grows homogeneously on Cu(111) terraces.

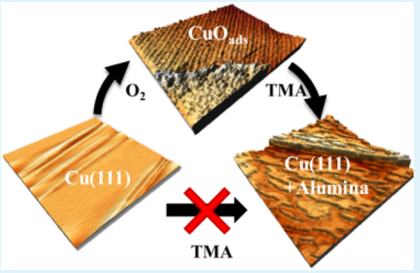

KEYWORDS: *Cu(111), trimethylaluminum (TMA), scanning tunneling microscopy (STM), X-ray photoelectron spectroscopy (XPS), high-resolution electron energy loss spectroscopy (HREELS), atomic layer deposition (ALD), surface science, single crystal*

INTRODUCTION

Copper is widely used for a variety of applications including water heat exchangers,[1] interconnect and gate electrodes for microelectronics,[2,3] and heterogeneous catalysts for reactions including low temperature water−gas shift (WGS)[4] and methanol steam reforming.[5,6] However, the use of copper in these applications is limited by corrosion in oxidative environments,[1,7] diffusion into adjacent layers in microelectronics,[2,8] and particle sintering and leaching in Cu-based catalysts.[6] Recently, atomic layer deposition (ALD) of alumina using trimethylaluminum (TMA) has been introduced to form protective coatings on Cu surfaces that prevent corrosion in oxidative environments,[1,7] diffusion of Cu in Cu_2S films in photovoltaic (PV) devices,[8] and sintering of Cu-based nanoparticles in liquid phase hydrogenation reactions.[6,9,10]

ALD is a variation of chemical vapor deposition (CVD) based on cyclic, self-limiting reactions of gaseous precursors with a solid surface.[11] For binary ALD reactions, each ALD cycle consists of two half-cycles during which the surface is consecutively exposed to a precursor and a coreactant. Between each cycle, the reaction chamber is purged by inert gas or vacuum. TMA is the most widely used ALD precursor for growth of aluminum oxide films, and water is one of the most common coreactants (see, for instance, reference 12 and references therein).

Received: April 25, 2015
Accepted: July 9, 2015
Published: July 9, 2015

DOI: 10.1021/acsami.5b03598
ACS Appl. Mater. Interfaces 2015, 7, 16428−16439

Though the interaction of TMA with adsorbed hydroxyl functional groups on Al has been studied in depth,[12] the reaction of TMA with air-exposed copper surfaces complicates this ideal ALD picture due to the formation surface oxides at room temperature.[13] Furthermore, this oxide persists and rearranges at 473−623 K to form the ordered "44" structure[12] on Cu(111), a structured Cu_2O overlayer with unit cell size 44 times larger than the Cu(111) unit cell. This temperature range corresponds to processing temperatures for TMA+H_2O ALD with the maximum growth rate.[14] This and other adsorbed oxygen structures persist on the surface until at least 773 K. Hydroxyl formation via water dissociation on copper surfaces is difficult. On Cu(111), thermally induced water dissociation was not observed in UHV.[15] No adsorbed hydroxyl species formed following exposure of clean Cu(111) to 1 Torr of water up to 333 K; however, a preoxidized Cu surface readily forms hydroxyls during water exposure at the same conditions.[16] In UHV, exposure of a preoxidized Cu(111) surface to 200 L H_2O at 1×10^{-6} Torr at 473 K resulted in a surface with both oxide (Cu_2O) and hydroxide patches.[17]

TMA+H_2O ALD performed on oxidized Cu surfaces has resulted in low growth per cycle during the first several cycles. Abdulagatov et al.[1] studied alumina ALD on copper oxide using TMA and water on an *in situ* copper-plated quartz crystal microbalance (QCM). They observed a nucleation delay at 450 K. The nucleation delay was caused by blockage of the copper oxide surface by carbonaceous species and/or lack of initial hydroxyl groups; however, the cause was not determined due to the lack of chemical information. Lu et al.[17] demonstrated that alumina grows preferentially on step edges of a partially hydroxylated, oxidized Cu(111) surface for TMA+H_2O ALD. They speculated from STM images that TMA reacts with OH but not copper oxide.

In this work, we sought to understand better the reactivity of TMA with copper oxide surfaces. More broadly, we sought to study the reactivity of TMA with copper oxide and alumina in the absence of a source of hydroxyl groups and to examine the resulting surface chemistry and morphology. The reaction of TMA with alumina has received attention in the literature;[14,18,19] however, here we used O_2 as the ALD coreactant rather than H_2O to isolate the interaction with the oxide and to exclude OH groups. We found that low carbon alumina films are possible using TMA+O_2 ALD, and that TMA reacts with oxygen in both alumina and copper oxide. The high growth rate of ∼3−4 Å/cycle was achieved on the surface with low carbon content.

O_3 and O_2 plasma are coreactants often used with TMA (see, for instance, reference 20 and references therein). Typically, electronic properties of Al_2O_3 films (charge density, recombination velocity, breakdown field, dielectric constant, etc.) are discussed and the quality of Al_2O_3 films is compared for different oxidants (O_3, O_2 plasma, or H_2O) in the literature. In a few publications, possible chemical mechanisms were discussed for "H_2O-free" ALD with TMA. On the basis of simulations, Elliott et al. supposed that the chemical mechanism of TMA+O_3 involved hydroxyl groups, which were produced on the surface by the oxidation of adsorbed methyl groups by O_3.[21] *In situ* FTIR studies of TMA+O_3 revealed that O incorporation into the surface results in a stable formate intermediate.[22] Aluminum methoxy, $-Al(OCH_3)_2$, and surface Al−O−Al linkages formed after O_3 pulses were suggested as reaction sites for TMA.[23] *In situ* attenuated total reflection Fourier transform infrared spectroscopy data show that both OH groups and carbonates were formed on the surface during the oxidation cycle of TMA+O_3 and TMA+O_2 plasma.[24] OH groups and C-containing impurities were found to be incorporated in the Al_2O_3 film during TMA+O_2 plasma ALD, and the impurity level could be reduced by prolonging the plasma exposure.[25,26]

To obtain direct chemical information and elucidate the reaction pathways of TMA with copper oxide and alumina without OH groups, we coupled surface-sensitive techniques including X-ray photoelectron spectroscopy (XPS) and high-resolution electron energy loss spectroscopy (HREELS) with scanning tunneling microscopy (STM) and density functional theory (DFT) modeling.

EXPERIMENTAL SECTION

Experiments were performed in an Omicron Surface Analysis Cluster at the Birck Nanotechnology Center (BNC) at Purdue University and at the ISISS beamline at the BESSY II synchrotron in Berlin, Germany. The Omicron Surface Analysis Cluster consists of an ultrahigh vacuum (UHV) preparation chamber and a μ-metal analysis chamber with base pressures of 1×10^{-9} and 5×10^{-11} mbar, respectively. The preparation chamber was equipped with a residual gas analyzer, an Ar^+ sputtering gun, resistive sample heating, and ALD precursor manifolds for precursor dosing, which are connected to the system via leak valves. The analysis chamber was equipped with XPS, HREELS, STM, low energy electron diffraction (LEED), and resistive sample heating. The sample temperature was measured by a K-type thermocouple attached to the sample holder.

STM images were obtained at room temperature in constant current (topographic) mode with electrochemically etched W tips. Etched W tips were conditioned in UHV by electron bombardment. STM images were analyzed using WSxM software.[27] STM height measurement was calibrated by setting the step height of a monatomic step on clean Cu(111) equal to 0.208 nm.

HREELS spectra were acquired using an ELS5000 instrument (LK Technologies) in the specular direction with primary beam energy of 5 eV. The resolution, measured as the full width at half-maximum (fwhm) of the elastic peak, was <3 meV (<24 cm^{-1}). All HREELS spectra have been normalized to the elastic peak intensity.

XPS data were acquired using a nonmonochromatic Mg Kα X-ray source ($h\nu$ = 1253.6 eV) with gun power of 150 W. High-resolution spectra were recorded at constant pass energy of 20 eV. The resolution, measured as the fwhm of the Cu $2p_{3/2}$ peak, was approximately 1.2 eV. Photoelectrons were collected at a photoemission angle of 45° with respect to the surface normal. Energy scale correction was not foreseen by the analyzer manufacturer (the electron energy analyzer, Omicron EAC 125 and the analyzer controller, Omicron EAC 2000); therefore, it was possible only to set the Au $4f_{7/2}$ peak at 84.0 eV by changing the spectrometer work function.

The basic design of the experimental apparatus at BESSY II has been described in detail previously.[28] It contained a load lock and *in situ* analysis cell connected to an energy analyzer spectrometer via differential pumping stages. The experimental procedures for sample preparation, TMA dosing, and data collection have been described in detail in our previous publication.[29]

XPS data were analyzed with CasaXPS (version 2.3.16dev85) software.[30] Cu 3s peaks were fitted using an asymmetric Gaussian/Lorentzian line shape with tail dampening (CasaXPS line shape = LF(1.2, 1.3, 15, 60)). Nonmetallic species of oxygen (O 1s) and aluminum (Al 2s) were fitted with symmetric Gaussian/Lorentzian line shapes (CasaXPS line shape = GL(30) or SGL(20)). The two most intense core level Al peaks, Al 2p and Al 2s, overlap with the Cu 3p and Cu 3s peaks, respectively, associated with the Cu(111) substrate. Therefore, Al 2s and Al 2p contributions were calculated from the curve-fitting.

To calculate coverage from XPS data, we followed Fadley's approach,[31] which assumes a nonattenuating adlayer at fractional coverage. Coverage (Θ), measured in monolayers (ML), is the ratio

DOI: 10.1021/acsami.5b03598
ACS Appl. Mater. Interfaces 2015, 7, 16428−16439

between the number of adsorbed species and the number of surface Cu atoms on (111) plane, and is expressed in eq 1:

$$\Theta = \frac{N_l(\theta) \times \Omega_s(E_s) \times A_S(E_s) \times \frac{d\sigma_s}{d\Omega} \times \Lambda_e^{subst}(E_s) \times \cos\theta}{N_s(\theta) \times \Omega_l(E_l) \times A_l(E_l) \times \frac{d\sigma_l}{d\Omega} \times d_s} \quad (1)$$

where $N_l(\theta)$ and $N_s(\theta)$ are the photoemission peak areas of the adlayer and the substrate at the given photoemission angle, θ, with respect to the surface normal; Ω is the acceptance solid angle of the electron analyzer; A_S and A_l are the effective substrate and adlayer area; $(d\sigma_l)/d\Omega$ and $(d\sigma_s)/d\Omega$ are differential cross sections for the photoemission peaks of the adlayer and the substrate, which are calculated using tabulated Scofield cross sections[32] and the Reilman asymmetry parameters;[33] $\Lambda_e^{subst}(E_s)$ is the electron attenuation length (EAL) of the photoelectrons originating from the substrate atom that have traveled through the substrate material; and d_s is the interlayer distance of the Cu(111) substrate. The EAL was calculated by NIST SRD-82.[34] Overlayer thicknesses were calculated using eq 2:

$$\frac{N_l(\theta)}{N_s(\theta)} = \frac{\rho_l \times \frac{d\sigma_l}{d\Omega} \times \Lambda_l(E_l)}{\rho_s \times \frac{d\sigma_s}{d\Omega} \times \Lambda_s(E_s)} \times \frac{\left(1 - \exp\left(\frac{-t}{\Lambda_l(E_l) \times \cos\theta}\right)\right)}{\left(\exp\left(\frac{-t}{\Lambda_l(E_s) \times \cos\theta}\right)\right)} \quad (2)$$

where ρ_l and ρ_s are the atomic densities of the overlayer and the substrate, respectively; $\Lambda_s(E_s)$ is the EAL of the photoelectrons originating from a substrate atom that have traveled through the substrate material; $\Lambda_l(E_l)$ is the EAL of photoelectrons originating from an overlayer atom that have traveled through the overlayer material; $\Lambda_l(E_s)$ is the EAL of photoelectrons originating from a substrate atom that have traveled through the overlayer material; and t is the overlayer thickness. All other variables are the same as in eq 1. XPS model derivations have been explained in detail in our previous publication.[35] eq 2 can be solved for t using the Thickness Solver tool.[36]

A Cu(111) single crystal disk with 10.0 mm diameter, 1.0 mm thickness (Princeton Scientific Corp.), and crystallographic orientation accuracy <0.5° was used. A polycrystalline Cu foil (Sigma-Aldrich, 99.99%) was used for the synchrotron experiments. Both samples were routinely cleaned by repeated cycles of Ar^+ sputtering and vacuum annealing at 1000 K. During the initial cleaning cycles, the Cu(111) crystal was treated in 5×10^{-6} mbar of O_2 at 623–673 K for 20 min to remove adventitious carbon. Single crystal cleanliness was monitored by XPS, STM, and LEED. No impurities (C, O, etc.) were detected by XPS on the Cu foil after cleaning procedures.

The Cu(111) crystal was exposed to TMA (Aldrich, 97%) in the preparation chamber via a leak valve at reported exposure values and temperatures. Prior to dosing TMA, several cycles of freeze–pump–thaw were performed for purification. Dosing lines were heated overnight at 423 K, and the lines were filled with TMA and pumped several times before dosing. Exposure values are reported in Langmuir (1 Langmuir = 1 L = 1×10^{-6} Torr·s), and pressures used to calculate exposures are taken from uncorrected ion gauge measurements. During TMA dosing, ionization gauges were left on for pressure measurement. Similar cycles of freeze–pump–thaw were performed on water ("Birck Nanograde Water", as SEMI E1.2 with the total organic carbon (TOC) reduced from 1 to 0.25 ppb). The water mini-cylinder was kept at room temperature during dosing. Separate dosing lines and leak valves were used for water to avoid cross contamination and accidental exposure of TMA to water in the dosing manifold.

Computational Methods. DFT calculations were performed by Vienna ab initio simulation package (VASP)[37] using projected augmented wave (PAW)[38] potential and PW91 exchange-correlation functional.[39] A plane wave cutoff of 400 eV was used. Cu(111) was modeled by a three-layer slab with (3 × 3) unit cell. The ordered Cu_2O layer grown on Cu(111) has a well-defined long-range structure in the literature consisting of Cu–O rings with isolated O located inside each ring.[13,40,41] The presence of this structure is confirmed by our STM images. To model this structure, a ring including 12 Cu and 13 O atoms on two-layer Cu(111) with (5 × 5) unit cell was used (Figure 1). The (4 × 4 × 1) and (2 × 2 × 1) k-point meshes were used to sample the Brillouin zone for Cu(111) and Cu_2O, respectively. The bottom-layer Cu atoms were fixed and the remaining atoms and adsorbates were relaxed until the residual forces less than 0.02 eV/Å. To prevent artificial interaction between the repeated slabs along the z-direction, 12 Å vacuum was introduced with correction of the dipole moment.

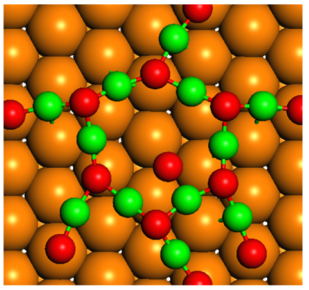

Figure 1. Optimized Cu_2O/Cu(111) structure. The orange, green, and red spheres represent Cu in Cu(111) lattice, Cu in the Cu_2O layer and O atoms, respectively. Atoms of the Cu_2O structure are scaled for visibility.

RESULTS AND DISCUSSION

Interaction of TMA and H_2O on Cu Foil. One goal of this work was to investigate the reactivity of TMA with copper oxide in the absence of hydroxyl groups. This was motivated by our previous research of TMA+H_2O ALD on Pt(111) and Pd(111).[29,42] In that work, aluminum hydroxide species were detected at <573 K in 0.1 mbar H_2O. These species dehydroxylated at higher temperatures. The hydroxide species gave rise to the Al $2p_{3/2}$ XPS peak at 74.9 eV, whereas alumina was characterized by a peak at 74.0 eV. Similarly, for *in situ*, synchrotron-based XPS of TMA+H_2O on Cu foil, the Al 2p BE shifted from ca. 75.1 eV after dosing TMA to 74.7 eV after dosing water at 473 K (Figure 2). The Al 2s peak showed the same trend. This BE shift is difficult to explain by the transformation of aluminum hydroxides to aluminum oxide and back: in 0.1 mbar H_2O, more hydroxide is expected than following TMA exposure, so a higher Al 2p BE under 0.1 mbar H_2O than after TMA exposure was expected, but the opposite trend was observed. To investigate possible alternative mechanisms of TMA interaction with Cu surfaces, we excluded the source of OH groups (H_2O) and other possible contaminants in the *in situ* cell by studying TMA+O_2 ALD under UHV conditions.

Interaction of TMA with Clean Cu(111). The interaction of TMA with clean Cu(111) was investigated after TMA exposure by XPS and HREELS. The Cu $2p_{3/2}$ and Cu 3s peaks obtained from clean, oxygen-free Cu(111) were located at 932.8 and 122.3 eV, respectively, both within 0.1 eV of literature-reported values for metallic Cu.[43] Figure 3 shows the Cu 3s/Al 2s XPS region obtained from the clean Cu(111) surface and following 2000 L TMA exposure at 473 K. No aluminum peaks, Al 2p or Al 2s, were observed by XPS following TMA adsorption on Cu(111). HREELS did not detect any characteristic vibrations of TMA or its fragments.[42] The absence of TMA adsorption on clean Cu(111) is in agreement with the findings of Lu et al.[17]

DFT calculations are also consistent with the lack of TMA adsorption on clean Cu(111). Figure 4 shows the free energy

DOI: 10.1021/acsami.5b03598
ACS Appl. Mater. Interfaces 2015, 7, 16428–16439

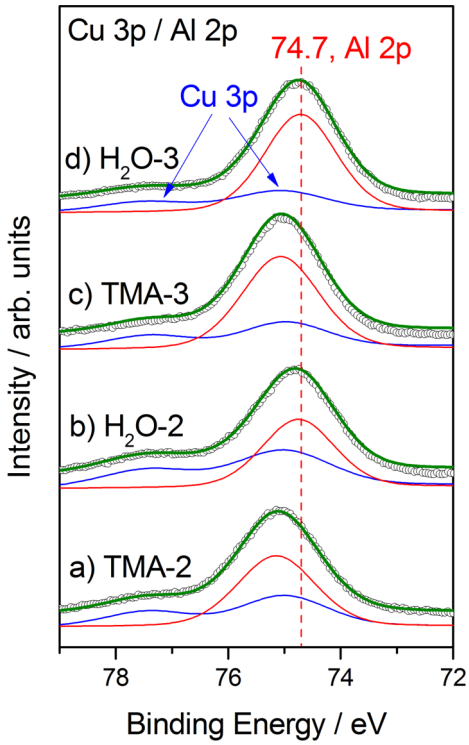

Figure 2. Cu 3p/Al 2p core-level regions obtained during TMA+H_2O ALD cycles on Cu foil by *in situ* XPS. (a) Second TMA half-cycle, (b) second H_2O half-cycle, (c) third TMA half-cycle, and (d) third H_2O half-cycle. TMA was exposed for 2000 L at ca. 373−473 K for all TMA half-cycles, and H_2O was dosed *in situ* at 473 K at 0.1 mbar for all H_2O half-cycles.

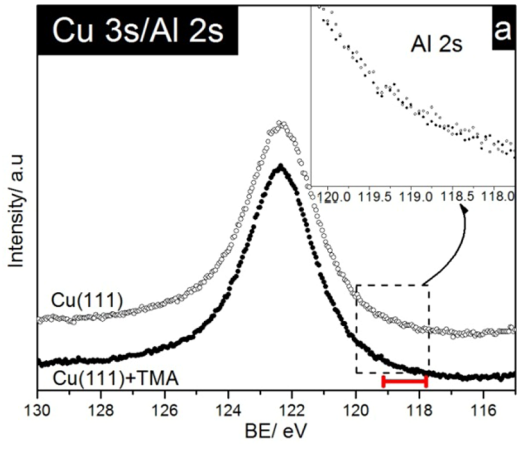

Figure 3. (a) Cu 3s/Al 2s XPS spectra obtained from clean Cu(111) (open circles) and from Cu(111) exposed to 2000 L TMA at 473 K (filled circles). The expected region for Al 2s is marked by the red bar. The inset shows the magnified Al 2s region.

diagram for dissociative TMA adsorption on Cu(111) at 473 K. The energy loss from the entropy of the gas-phase TMA (g) at 473 K and standard pressure was 0.84 eV and the binding energy of TMA adsorbed on Cu(111) was −0.28 eV (computational details regarding entropy changes associated with precursor adsorption can be found in reference 44). Therefore, the difference between the free energy level of TMA (g) and TMA* was +0.56 eV. This means that TMA adsorption on Cu(111) is endothermic. TMA dissociation on clean Cu(111) was also found to be endothermic: the calculated

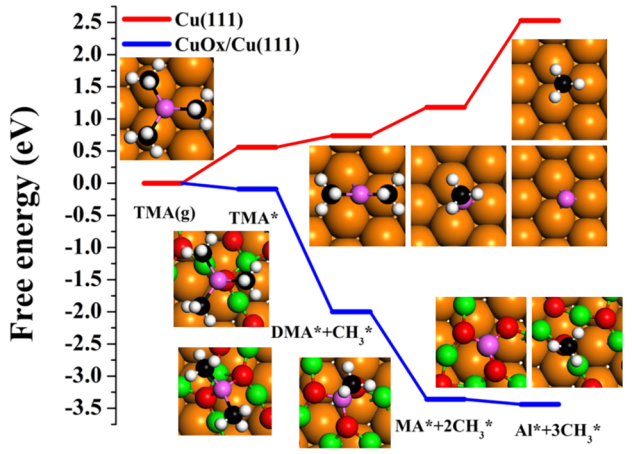

Figure 4. Free energy diagrams of TMA dissociation on Cu(111) and Cu_2O/Cu(111). The insets are the optimized most stable structures of adsorbed TMA, dimethylaluminum (DMA), methylaluminum (MA), Al, and CH_3, respectively. The orange, green, pink, black, red, and white spheres represent Cu of Cu(111), Cu of Cu_2O, Al, C, O, and H atoms, respectively.

energies for dissociative reactions of TMA to dimethylaluminum (DMA), DMA to methylaluminum (MA), and MA to Al and CH_3 were 0.17, 0.45, and 1.35 eV, respectively.

Preparation of Cu_2O/Cu(111). Oxygen was adsorbed on Cu(111) by exposure to 4500 L O_2 at 623 K. O 1s, Al 2s, and C 1s XPS core-level regions obtained from the Cu_2O/Cu(111) surface are shown in Figure 5, and STM images are presented in Figure 6. The O 1s peak was fitted with one component at 529.8 eV, which was assigned to oxygen in the Cu_2O layer (assignment made by STM below). Reported Cu_2O BEs range from 529.9 to 531.0 eV (see reference 45 and references therein). A high BE shoulder at ca. 936.0 eV was observed in the Cu $2p_{3/2}$ core-level region following oxygen exposure indicating that some Cu_2O was present (data shown in Supporting Information Figure S1). The Cu 3s/Al 2s region was unaffected by the first O_2 exposure. Neither XPS nor HREELS of this surface revealed any hydroxyl species (HREELS spectrum shown in Supporting Information Figure S2). It should be noted that Al 2s was used instead of Al 2p for UHV XPS experiments due to the overlap of Al 2p with Cu 3p.

Figure 6a shows STM images of clean Cu(111), and Figure 6b−e shows Cu(111) following oxygen exposure. The step edges of the clean Cu(111) surface are smooth with step height of 0.21 nm. After oxygen exposure at 623 K, a sawtooth pattern is observed on the steps (Figure 6b), and a well-ordered oxide structure is observed on terraces (Figure 6c−e). After annealing oxygen-exposed Cu(111) surfaces at 473−623 K, Matsumoto et al.[13] observed the well-ordered "44" structure, which consists of 7 hexagonal O−Cu−O rings in a unit cell 44 times larger than the (1 × 1) unit cell of Cu(111). This superficial oxide has stoichiometry Cu_2O. A scheme of the 7 rings is shown overlaying our STM image in Figure 6e.

The assignment to Cu_2O is based on STM images showing the "44" structure and lack of pronounced XPS shakeup in the Cu 2p region. We cannot rule out the presence of small amounts of Cu^{2+} given the surface sensitivity of our instrument. After O_2 half-cycles, we do see slight broadening of the Cu 2p peak high BE side (shown in Supporting Information Figure S1), which might be indicative of the formation of some Cu^{2+}.

DOI: 10.1021/acsami.5b03598
ACS Appl. Mater. Interfaces 2015, 7, 16428−16439

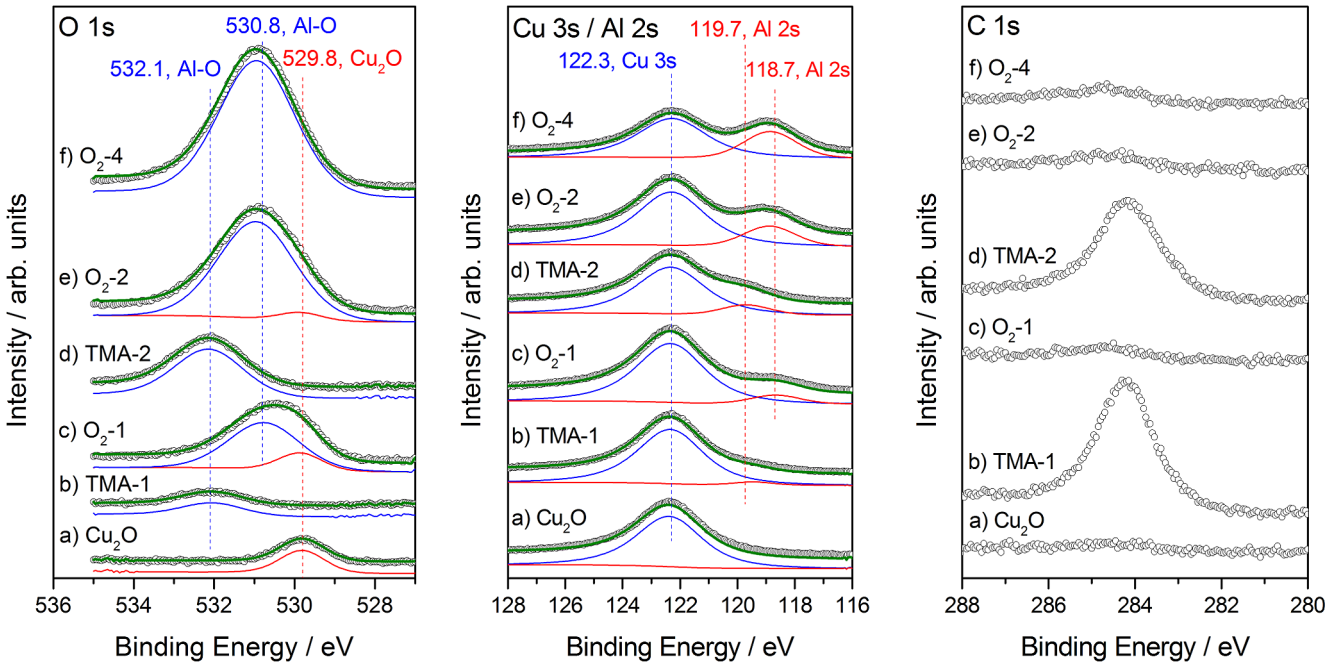

Figure 5. O 1s, Cu 3s/Al 2s, and C 1s XPS core-level regions obtained (a) from Cu_2O/Cu(111) (4500 L O_2 at 623 K), (b) after the first TMA half-cycle, (c) after the first O_2 half-cycle, (d) after the second TMA half-cycle, (e) after the second O_2 half-cycle, and (f) after four complete ALD cycles. TMA was exposed for 2000 L at 473 K for all TMA half-cycles, and O_2 was exposed for 4500 L O_2 at 623 K for all O_2 half-cycles. The apparent increase in Al 2s peak intensity after O_2 half-cycles relative to TMA cycles is due to the removal of carbon.

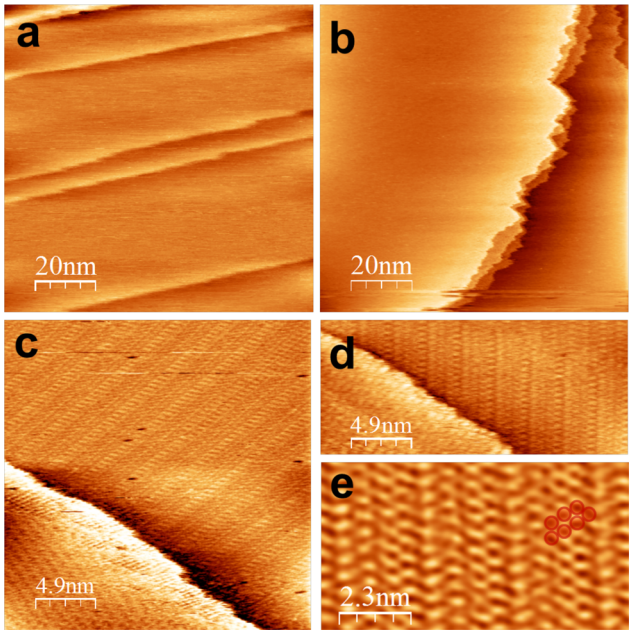

Figure 6. STM images of (a) clean Cu(111) and (b–e) Cu(111) exposed to 4500 L O_2 at 623 K. The seven rings of Cu_2O with the "44" structure[13] are shown in image e. Bias voltages were −0.5 V for all images, and tunneling currents were 0.5 nA (images a, b) and 1.0 nA (images c–e). Image e was processed using a wavelet filter in WSxM Software;[27] see the Supporting Information for more details.

Cu^+ and Cu^0 are difficult to separate from the Cu 2p core-level, as their range of reported binding energies overlap.[43]

First TMA Half-Cycle. Figure 7 shows the HREELS spectrum obtained after Cu_2O/Cu(111) was exposed to 2000 L TMA at 473 K. Major peaks were detected at 608, 747, and 882 cm^{-1}, and weaker peaks were detected at ca. 1480, 1645, and 1750 cm^{-1}. The peak at 608 cm^{-1} (ν_1) was assigned to the group of stretching vibrations between tetrahedrally coordinated Al^{3+} cations (A_{tet}) and their four nearest O^{2-} neighbors, the peak at 880 cm^{-1} (ν_3) was due to the group of stretching vibrations between octahedrally coordinated Al^{3+} cations (Al_{oct}) and their six nearest O^{2-} neighbors (ν_3), and the peaks at 1480 and 1750 cm^{-1} correspond to $\nu_1+\nu_3$ and 2 ν_3 multiple loss events, respectively.[46,47]

The ratio of the peak areas of tetrahedral to octahedral Al^{3+}, Al_{tet}/Al_{oct}, (Figure 7) was 0.27. The peak at 740–770 cm^{-1} (ν_2) (and the multiple loss event peak $\nu_2+\nu_3$ at 1645 cm^{-1}) was not assigned. Other weak peaks that appeared at 1215 and 2920 cm^{-1} likely were $\delta_s(CH_3)$ and $\nu_{s/as}(CH_3)$ signatures, respectively, of methyl groups attached to the copper surface.[48,49] Indeed, DFT predicted that methyl ligands were transferred from Al center to the copper surface (Figure 4). However, dehydrogenation of the $CH_{3,\,ads}$ species could not be ruled out: the peak at 2920 cm^{-1} was broad and it might be characteristic of other $CH_{x,\,ads}$ species such as CH_{ads} and $CH_{2,\,ads}$. The corresponding deformation vibrations, $\delta_s(CH_x)$, likely overlapped with intense ν_1, ν_2, ν_3 and multiple losses. Nominal carbon coverage was approximately 1.0 ML.

We did not observe a loss peak at ca. 400 cm^{-1} that has been assigned previously to vertical Al–O vibrations between in-phase alumina layers on different metal surfaces.[46] This supports the assignment of monolayer growth during the first cycle. As shown in Figure 6, the ratio of ν_1 to ν_3 (tetrahedral to octahedral) peak areas was 0.27.

After TMA was dosed to the Cu_2O/Cu(111) surface, the XPS O 1s peak shifted from 529.7 to 532.1 eV (Figure 5) and the shoulder of Cu $2p_{3/2}$ at 936.0 eV disappeared, revealing that oxygen adsorbed on Cu was incorporated into the newly formed adlayer structure. Similarly, surface oxides have been reduced on GaAs and Ge(100) substrates during TMA exposure.[50,51] The Al 2s contribution to the Al 2s/Cu 3s

DOI: 10.1021/acsami.5b03598
ACS Appl. Mater. Interfaces 2015, 7, 16428–16439

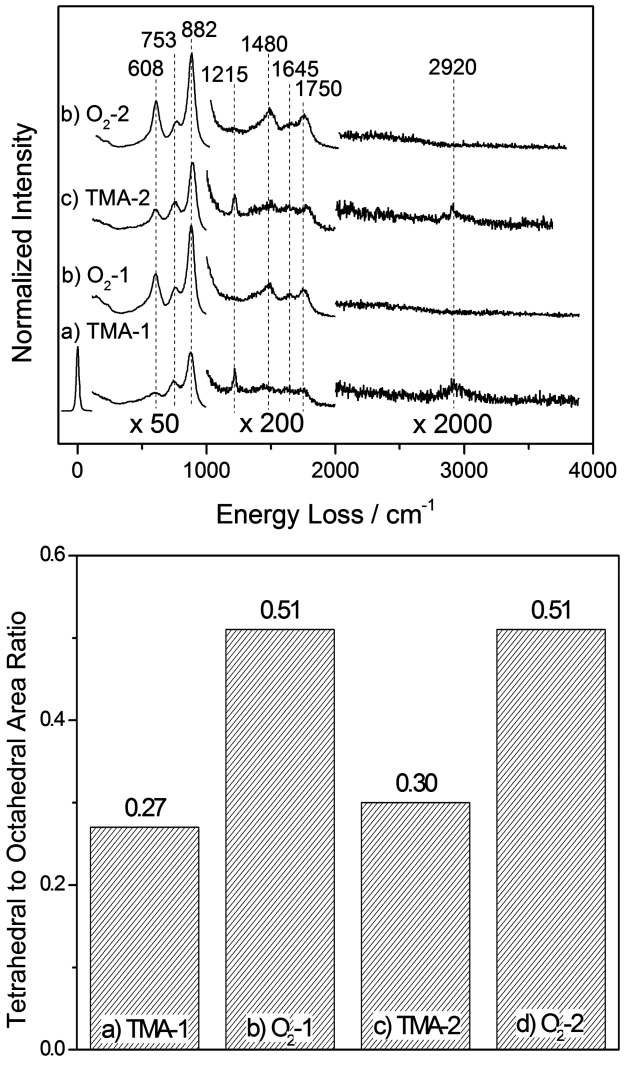

Figure 7. Top: HREELS spectra obtained after (a) first TMA half-cycle, (b) first O_2 half-cycle, (c) second TMA half-cycle, and (d) second O_2 half-cycle. Bottom: area ratio between ν_1 and ν_3 peaks (Al_{tet}/Al_{oct}) for each TMA and O_2 half-cycle. TMA was exposed for 2000 L at 473 K for all TMA half-cycles, and O_2 was exposed for 4500 L O_2 at 623 K for all O_2 half-cycles.

peak envelope was observed at ca. 119.5 eV (Figure 5b). The O 1s (Al−O contribution) and Al 2s peak areas were used to calculate O and Al atomic percentages. The resulting Al:O atomic percentage ratios are plotted for each O_2 half-cycle in Figure 8. For the first TMA half-cycle, the Al:O ratio was approximately 0.46. Stoichiometric Al_2O_3 would yield an Al:O ratio of 0.66. This Al:O ratio of approximately 0.5 suggests the presence of a copper aluminate, for example $CuAlO_2$.

STM images of the TMA-exposed surface (Figure 9) reveal two-dimensional (2D) islands on the surface with an average height of approximately 0.19 nm (a pixel height histogram was used for island height estimation and is shown in Supporting Information Figure S3). No long-range order of the copper surface oxide was observed. The bimodal peak distribution in the height histogram confirmed that the islands are flat with uniform height. Some defects (shown by black arrows in Figure 9b) were observed.

TMA adsorption and dissociation on the $Cu_2O/Cu(111)$ surface was found to be exothermic (Figure 4). TMA tends to adsorb at the top position on O in the Cu−O ring via an Al

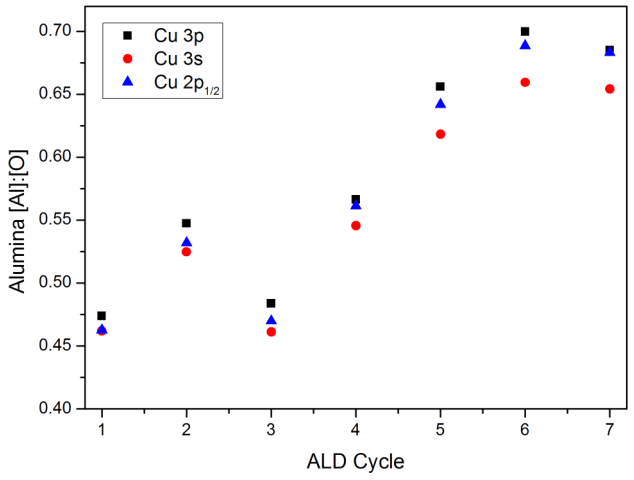

Figure 8. Alumina Al:O atomic percentage ratio versus ALD cycle number. TMA was exposed for 2000 L at 473 K for all TMA half-cycles, and O_2 was exposed for 4500 L O_2 at 623 K for all O_2 half-cycles. Atomic percentages were calculated using Cu 3p (black square), Cu 3s (red circle), and Cu $2p_{1/2}$ (blue triangle) peaks for comparison. In all cases, the Al 2s peak and Al−O component of the O 1s peak were used in the atomic percentage calculation.

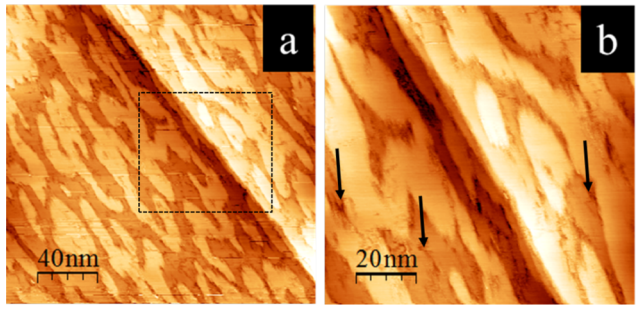

Figure 9. STM images of the $Cu_2O/Cu(111)$ surface exposed to 2000 L TMA at 473 K (a) 200 nm × 200 nm and (b) 100 nm × 100 nm. The tunneling current was 1.0 nA; the bias voltage was −0.75 V.

atom with a binding energy of −0.93 eV, which is stronger by 0.65 eV compared to adsorption on clean Cu(111). The free energy for TMA dissociation to DMA is −1.91 eV, and the formed DMA is bound to the bridge site of two adjacent O atoms in the Cu−O ring. DMA dissociation to MA is exothermic by −1.36 eV, and the Al atom of MA coordinates with three O atoms including the isolated O inside the ring. The final step considered, MA dissociation to Al and CH_3, is exothermic by −0.09 eV, and the formed Al atom is bound to three O atoms. The exothermicity of dissociative TMA adsorption on the $Cu_2O/Cu(111)$ surface is the result of high binding energies of the intermediates on this surface. Compared with clean Cu(111), the binding energies of DMA, MA, Al, and CH_3 are stronger on $Cu_2O/Cu(111)$ by 2.19, 3.45, 4.35, and 0.54 eV, respectively. In conclusion, DFT calculations predicted no TMA adsorption on Cu(111) but TMA adsorption and dissociation on $Cu_2O/Cu(111)$, consistent with experimental data.

Both experiments and first-principles calculations demonstrate that TMA is capable of reacting with a copper oxide surface in the absence of hydroxyl species. The reaction of TMA with the $Cu_2O/Cu(111)$ layer is limited by the initial amount of oxygen present in the Cu_2O lattice and as trace CuO. TMA consumes oxygen from the surface oxide and

DOI: 10.1021/acsami.5b03598
ACS Appl. Mater. Interfaces 2015, 7, 16428−16439

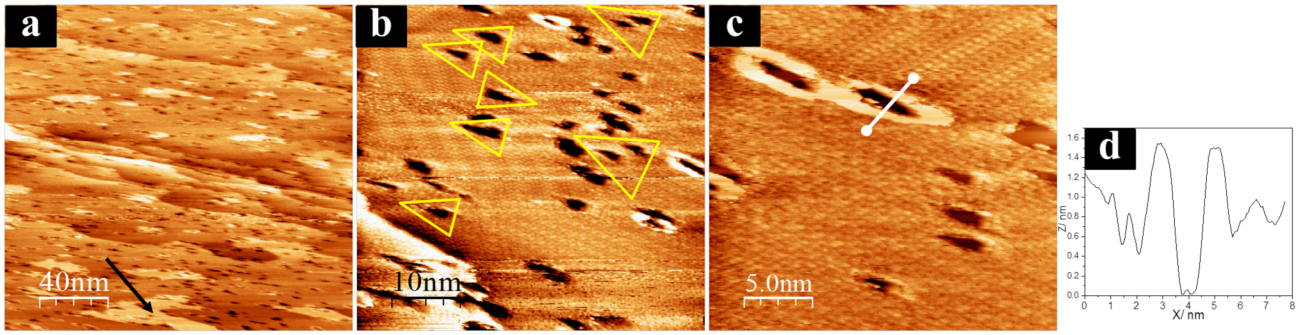

Figure 10. STM images after first O_2 half-cycle (4500 L O_2 at 623 K) (a) 200 nm × 200 nm, (b) 50 nm × 50 nm, and (c) 25 nm × 25 nm. (d) Line profile along the solid white line indicated in image c. I_t = 1.0 nA, U_t = −0.75 V.

reduces oxidized Cu to the metallic state, as evidenced by the lack of long-range order in STM images and the shift in the O 1s XPS peak following the TMA half-cycle. Once the substrate is reduced to Cu^0, the surface is inactive for further TMA adsorption and decomposition. As evidenced by the partial monolayer film growth, oxygen must migrate across the surface, forming adlayer islands. On the basis of the Al:O ratio of 0.46, these islands are most likely $CuAlO_2$. The island height of 0.19 nm is close to the reported Cu−O and Al−O bond lengths of 1.861 and 1.912 Å, respectively, in $CuAlO_2$ crystalline.

On the basis of the data discussed above, a simplified stoichiometric equation of TMA reaction with on Cu_2O/Cu(111) can be proposed:

$$2Cu_2O + Al(CH_3)_3 \rightarrow CuAlO_2 + 3Cu + 2CH_4\uparrow + CH_{ads} \quad (3)$$

TMA adsorption is limited by the amount of the surface oxygen. The island formation during TMA dosing can be explained by the difference of surface atomic densities of the reactant and products in eq 3. The density of surface copper atoms in the "44" structure is approximately 2 times lower than the corresponding value for Cu(111), meaning that 2 Cu_2O units cover an area of 8 Cu atoms in the Cu(111) terrace. Three cooper atoms and $CuAlO_2$ cannot compensate the area of 2 Cu_2O, and this leads to the island formation as shown in Figure 9. The transformation of hydrocarbon products is not straightforward. HREELS revealed methyl groups on the surface. On the other hand, methyl group dehydrogenation could not be ruled out.

First O_2 Half-Cycle. Following TMA exposure to the Cu_2O/Cu(111) surface, O_2 was exposed to the resulting surface for 4500 L at 623 K. The HREELS spectrum obtained from this surface is shown in Figure 7b. Compared to the first TMA half-cycle, the intensity of the peak at 608 cm^{-1} related to Al_{tet} increased, and the Al_{tet}/Al_{oct} intensity ratio was equal to 0.51 (Figure 7). The $\delta_s(CH_3)$ and $\nu_{s/as}(CH_3)$ vibrations of the $CH_{3,ads}$ groups on Cu(111) disappeared, but a weak C 1s peak slightly shifted to higher BE was detected by XPS (Figure 5). The fact that there was more octahedral Al^{3+} present after the TMA cycle than after the O_2 half-cycle could be due to the formation of $CuAlO_2$ after the TMA half-cycle, in which Al^{3+} cations are octahedrally coordinated.[51]

Curve-fitting of the O 1s peak revealed two components: the component at 529.9 eV represents Cu_2O (19% of the total O 1s area) and the second component at 530.8 eV is from oxygen in the copper aluminate (81% of the total O 1s area) (Figure 5). An O 1s BE of 531.2 eV has been reported previously for thin film alumina on Pt(111).[29] The slight Cu $2p_{2/3}$ peak shoulder reappeared at ca. 936.0 eV, consistent with the formation of some CuO (see Supporting Information Figure S1). Cu_2O was also formed, as evidenced by long-range order observed in STM images (Figure 10b,c). The Al 2s peak is distinguishable from the shoulder of Cu 3s at 118.7 eV (Figure 5). Al 2s shifted by −0.8 eV to 118.7 eV following O_2 exposure. Lower Al 2p binding energies for aluminum oxides have been attributed to the presence of Al^{3+} coordinated tetrahedrally[52−55] (see discussion in reference 29). In this case, the Al 2p and Cu 3p peaks overlap, but the Al 2s and Al 2p peaks should exhibit a similar chemical shift in XPS. Here, the shift to lower BE is consistent with the formation of alumina with an increased Al_{tet}/Al_{oct} ratio following the O_2 half-cycle. A hydroxide-containing species can cause a similar shift of the O 1s and Al 2p (Al 2s) peaks;[56−58] however, no O−H stretching vibrations were detected by HREELS after TMA or O_2 half-cycles at ca. 3300−3700 cm^{-1}. The Al:O ratio after the first O_2 half-cycle was approximately 0.53, nearly unchanged from after the first TMA cycle. The resulting Al:O atomic percentage ratios after each O_2 half-cycle are plotted in Figure 8.

Figure 10 shows STM images of the copper surface after the first O_2 half-cycle. As evidenced by the well-ordered Cu_2O structure that can be seen in atomic-resolution images (Figure 10b,c), O_2 exposure reoxidizes the copper surface. Two other features are observed: Aluminum oxide islands that appeared after the first TMA half-cycle with an average height of 0.17 nm (marked by black arrow in Figure 10a), and dark spots appeared on the Cu terrace. Obtaining STM images over regions with a high density of aluminum oxide islands was problematic due to the low density of states for achieving a stable tunneling current and therefore was avoided. Dark spots with a triangular shape are marked inside yellow lines in Figure 10b. As shown by Matsumoto et al.,[13] oxygen is capable of abstracting Cu from terraces and leaves behind triangular holes with the 3-fold symmetry. Some of these pits are decorated with bright features (apparent height of ∼1.5 nm, Figure 10c,d). These features could be Cu adatoms from the oxide structure that became mobile and diffused across the surface until reaching a low-coordination site such as a hole. The holes detected by STM are likely "mines" delivering copper to the surface, as has been observed for Ag in the Cu/Ag(111) system.[59]

A simple mechanism for the O_2 half-cycle can be proposed:

$$2Cu + 2CuAlO_2 + 2CH_{ads} + 3O_2 \rightarrow 2Cu_2O + Al_2O_3 + 2CO_2\uparrow + H_2O\uparrow \quad (4)$$

DOI: 10.1021/acsami.5b03598
ACS Appl. Mater. Interfaces 2015, 7, 16428−16439

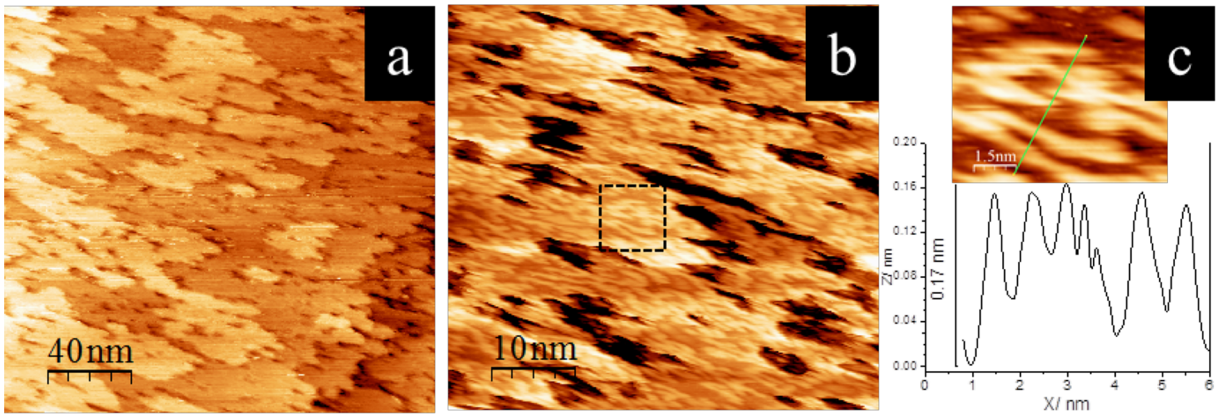

Figure 11. STM images (a) 200 nm × 200 nm and (b) 50 nm × 50 nm obtained after the second TMA half-cycle (2000 L TMA at 473 K). (c) Zoom-in region of the highlighted section in image b and the line profile along the solid line indicated in the image. The tunneling current was 0.5 nA; the bias voltage was −0.9 V.

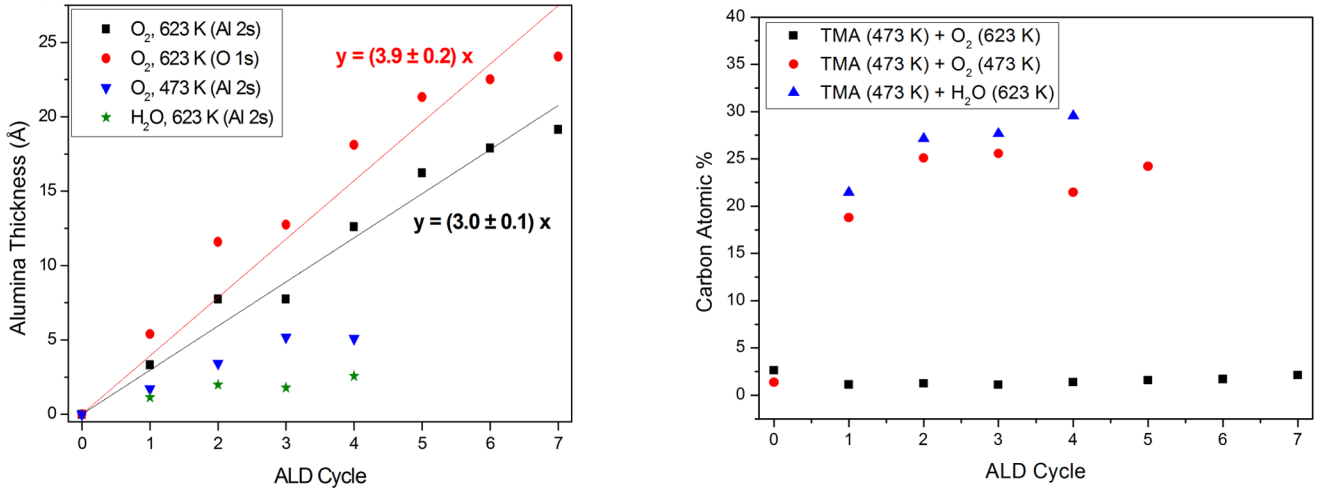

Figure 12. Left: nominal alumina thickness versus ALD cycle for various coreactant dosing conditions. Dosing conditions were O_2, 623 K (black squares, calculated using Al 2s; red circles, calculated using O 1s), O_2, 473 K (red triangles, calculated using Al 2s), and H_2O, 623 K (green stars, calculated using Al 2s). Right: carbon atomic percentage for various coreactant dosing conditions.

Copper is reoxidized forming the $Cu_2O/Cu(111)$ structure, as shown in Figure 10. Because the Cu_2O structure has a lower density of copper atoms than a Cu(111) terrace, Cu_2O formation results in "swelling" the surface and the islands become masked. The $CH_{x,ads}$ species reacts with oxygen and desorbed as CO_2 and H_2O. The recombination of $CH_{x,ads}$ to C_2 and C_3 products cannot be ruled out completely, but this process should be unfavorable in the presence of oxygen. The role of copper is to provide dissociation sites for O_2 adsorption and dissociation. The transformation of $CuAlO_2$ to Al_2O_3 was not confirmed but it can explain the changing ratio of tetrahedral to octahedral HREELS peak areas.

Second ALD Cycle. Figure 11 shows STM images obtained after the second TMA half-cycle. Numerous holes were seen on terraces and islands. Terraces were covered with islands having sharp boundaries and a ridge-like structure (marked by a rectangle in Figure 11b,c). These morphological changes reflected the transition from monolayer alumina islands after the first TMA half-cycle (Figure 9) to multilayer islands, as the ridge structure is likely the second alumina layer and/or $CuAlO_2$. The ridges have an apparent height of about 0.17 nm (Figure 11b), close to the average height for the alumina islands (0.19 nm) after the first TMA half-cycle observed in Figure 9.

Similar to the first TMA half-cycle, TMA consumed oxygen from the Cu_2O structure and reduced Cu oxide to Cu^0 as evident from the disappearance of long-range ordered Cu_2O structures in STM images. Unlike the first TMA half-cycle, growth is not limited to the copper oxide surface as existing alumina islands can serve as the oxygen source. TMA reduces the aluminum oxide layer wherever the two are in direct contact.

After the second O_2 half-cycle, the Al 2s and O 1s peaks were shifted toward lower BEs at 118.9 and 531.0 eV, respectively (Figure 5). As discussed above, these peaks are characteristic of the alumina structure with the Al_{tet}/Al_{oct} HREELS peak area ratio of ~0.5 (Figure 7 inset). The Cu_2O contribution in the O 1s peak was one-quarter the size (5% of the O 1s area) of the corresponding value observed after the first O_2 half-cycle, which reflected the decrease in the copper surface available for oxygen adsorption. Most carbon was removed after the second O_2 half-cycle (Figure 5), consistent with disappearance of the $\delta_s(CH_3)$ and $\nu_{s/as}(CH_3)$ peaks in the HREELS spectrum (Figure 7).

Subsequent ALD Half Cycles and Film Growth Behavior. Seven ALD cycles (14 half-cycles of O_2 and TMA) were performed on the $Cu_2O/Cu(111)$ surface (Figure 12). Each TMA half-cycle consisted of 2000 L TMA at 473 K

DOI: 10.1021/acsami.5b03598
ACS Appl. Mater. Interfaces 2015, 7, 16428−16439

and each O_2 half-cycle consisted of 4500 L O_2 at 623 K. Nominal alumina thicknesses calculated from the Al 2s and O 1s peaks are plotted in Figure 12. Roughly linear alumina growth is observed during the first 7 ALD cycles. The nominal calculated thickness gain per cycle using the Al 2s and O 1s peaks, respectively, were 3.0 ± 0.1 and 3.9 ± 0.2 Å. From STM images, we conclude that Al deposition occurred on the surface with Cu_2O available and then the process proceeded on porous alumina once all Cu was covered. At the oxygen conditions used (623 K, 4500 L, 5×10^{-6} mbar), the carbon atomic percentage (calculated using the C 1s and Cu 3s regions) was equal to or less than 2 at. % for all ALD cycles. DFT calculations demonstrated that O_2 dissociates on Cu(111) to atomic oxygen.[60] This reactive atomic oxygen reacts with carbon clusters or methyl groups.

Figure 13 plots O 1s and Al 2s BEs after each TMA and O_2 half-cycle. The common behavior of the O 1s and Al 2s peaks

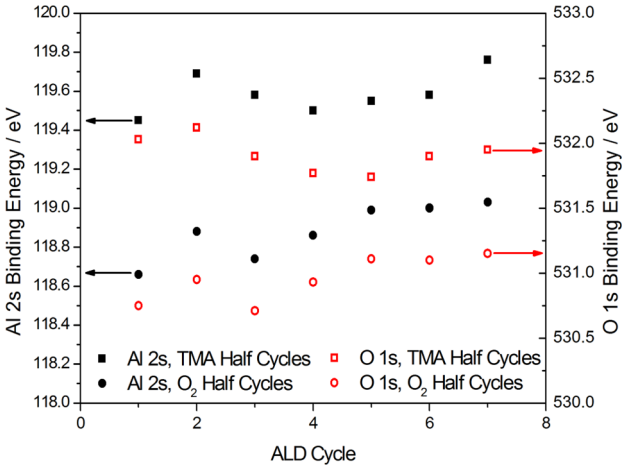

Figure 13. BEs of O 1s (red outlines) and Al 2s (solid black) peaks after each half-cycle of TMA or O_2. Squares were data points taken after TMA half-cycles, and circles were data points taken after O_2 half-cycles. Seven cycles in total were performed. The starting surface was the Cu_2O/Cu(111) surface.

was the shift to higher BE values after TMA half-cycles and the shift to lower BE values after O_2 half-cycles. On the basis of HREELS data from the first two cycles, these changes resulted from the transition between the octahedral and tetrahedral coordination of aluminum cations. The Al_{oct} contribution increased during TMA half-cycles, and the Al_{tet} contribution increased during O_2 half-cycles.

Figure 12 also shows nominal alumina thicknesses and carbon atomic percentages after each ALD cycle for a variety of coreactant dosing conditions. In all cases, the first TMA half-cycle was performed over Cu(111) exposed to O_2 for 4500 L at 623 K to form Cu_2O. For TMA+O_2 ALD, when the O_2 half-cycle was done at 473 K rather than 623 K, oxygen was not as effective in carbon removal. The carbon atomic percentage increased after each ALD cycle. After four ALD cycles at 473 K, nominal carbon coverage was about 10 times higher than for the O_2 half-cycle at 623 K. Alumina growth observed for the O_2 half-cycles at 473 K was much slower at these conditions, with a measured nominal thickness of ca. 5 Å after 4 ALD cycles, compared to ca. 15 Å after 4 cycles with O_2 dosing at 623 K. This slower growth is likely due to poisoning of the surface by carbon species.

To evaluate the effectiveness of the second reactant in carbon removal and alumina growth, O_2 was replaced with water dosed at 623 K, as shown in Figure 12. The water half-cycles were also ineffective for carbon removal. After four ALD cycles the carbon atomic percentage was ~30%. After one H_2O ALD cycle at 473 K, the nominal alumina thickness was about 3 Å, and the thickness did not increase for subsequent cycles. It must be noted that carbon removal behavior at the dosing pressures of O_2 and H_2O used in this study (~10^{-6} mbar) may not be representative of the same ALD process carried out in a typical ALD reactor at pressures of a few millibars.[29] On the other hand, we observed carbon accumulation on Cu foil during TMA+H_2O ALD *in situ* using synchrotron-based XPS at 473 K and 0.1 mbar H_2O pressure.

For ideal alumina ALD using H_2O as the coreactant, methyl ligands from TMA are partially exchanged with surface hydroxyl groups and the precursor becomes anchored to the surface during the first TMA half-cycle. Ideally, the coreactant provides the missing element (oxygen), removes the carbon groups via hydrogen transfer to CH_3, and functionalizes the surface for the upcoming TMA half-cycle. However, as demonstrated, this ideal picture is not always fulfilled, as TMA fully decomposes and forms an aluminate by losing all its methyl ligands upon deposition on a hydroxide-free Cu_2O surface at 473 K. TMA decomposition leaves behind carbon atoms and clusters, and methyl groups attached to the copper surface. Once the copper surface is completely covered, TMA continues to react with hydroxide-free alumina.

Others have studied the reaction of TMA with oxide-terminated alumina. Dillon et al.[18] observed the appearance of IR features assigned to CH_3 stretching following a saturation exposure of TMA to a porous alumina membrane previously annealed to 1000 K. These IR features had an integrated absorbance equal to 72% of the same features following exposure of an alumina surface with a saturation amount of hydroxyl. These CH_3 stretching features attenuated upon annealing between 300 to 860 K.[18] Puurunen et al.[19] found that TMA reacted between 353 and 573 K with alumina pretreated between 473 and 1073 K. TMA decomposed above 600 K. Assuming that all TMA reacts with hydroxyl groups, releases methane, and forms OAlMe species, the amount of carbon observed on the alumina with the highest pretreatment temperatures was higher than expected based on this assumption, suggesting that TMA adsorbs dissociatively on coordinatively unsaturated Al. They found that the amount of methyl groups present on alumina pretreated at 1073 K was 15% less than on alumina treated at 473 K. Elliott et al.[14] showed with first-principles calculations that TMA will chemisorb on both bare alumina and hydroxylated surfaces, that hydroxyl coverage does not affect site density, and that adsorbed TMA dissociates to form $AlMe_2$, AlMe, and Me on both surfaces. However, the hydrogen in OH^- reacts with methyl groups and CH_4 is evolved, so the ALD rate, which is affected by steric hindrance of CH_3 groups, is greater on hydroxylated surfaces. The findings shown here agree with the above authors.

The temperature of the surface during oxygen exposure plays an important role in the carbon removal and alumina growth behavior. Incorporation of impurities including carbon is a major concern in oxide dielectrics where an ultrathin film (<10 nm) is deposited by ALD. This application requires a carbon-free oxide film to achieve high-quality microelectronic devices.[61]

DOI: 10.1021/acsami.5b03598
ACS Appl. Mater. Interfaces 2015, 7, 16428−16439

As shown in Figure 8, the Al:O ratio is close to 0.5 for the first 3−4 ALD cycles before increasing and remaining steady at about 0.66. This transition in stoichiometry corresponds to the film closure. As shown in the O 1s region in Figure 5, the Cu−O peak from the Cu_2O surface oxide is no longer present after 4 ALD cycles. In the first several ALD cycles, the Al:O stoichiometry of 1:2 is due to the presence of $CuAlO_2$. There is more octahedral alumina after the early TMA cycles, because Al occupies the octahedral sites in $CuAlO_2$.[51] The presence of copper in the first few cycles forces Al into the octahedral positions. As the film closes and Cu is covered, the stoichiometry shifts to that of alumina, Al_2O_3. Alumina interacts with Cu at the interface. Though HREELS data for cycles beyond the second cycle were not collected, amorphous alumina is likely formed by ALD at these conditions.

Finally, we must note that the growth rates measured for TMA+O_2 ALD in this study are likely to differ from growth rates for the same process carried out at millibar pressures in a flow reactor. Because the focus of this study is on the first several ALD cycles, the Cu substrate may affect film growth even after film closure. The cleanliness of surfaces studied here is likely superior to those used for a typical ALD flow reactor, where contaminants may block ALD nucleation sites and often surface sensitive techniques to measure contaminant levels are not available. Finally, the high vacuum dosing pressures used in this study could alter the growth rate.

CONCLUSION

We have shown with surface sensitive characterization techniques and DFT calculations that TMA does not react with or adsorb on metallic Cu(111), but that TMA adsorption and decomposition to Al are thermodynamically favorable on Cu_2O. During the first half-cycle, TMA reacts with O adsorbed on Cu(111), depositing Al in the form of single layered aluminate islands. This reduces surface copper not bound to the aluminate to the metallic state, which does not interact with TMA. Therefore, the amount of adsorbed O limits the growth of Al during the first half-cycle.

From XPS and HREELS, TMA half-cycles favor production of octahedrally coordinated alumina, whereas O_2 half-cycles at higher temperature favor production of alumina in tetrahedral coordination. During the first ∼3 cycles while Cu is still exposed, XPS can differentiate between O in Cu_2O and $CuAlO_2$, and TMA interacts with both Cu_2O and the aluminate. TMA continues to interact with the aluminate/alumina once Cu is completely covered.

The choice of processing conditions in high vacuum determines the extent of carbon incorporation in the ALD film. Dosing TMA at 473 K and O_2 at 673 K results in a film with less carbon than when H_2O is used instead of O_2 at the same temperature, and for O_2 at 473 K. These alternative processing conditions result in increasing C deposition with each ALD cycle and little or no Al adsorption after about the third ALD cycle.

We have demonstrated that TMA readily reacts with oxide surfaces even in the absence of coadsorbed hydroxyls. For ALD applications on an air-exposed Cu surface, large domains of oxides might still exist. This is of great importance to thin film applications like microelectronics and catalysis where only a few ALD cycles are desirable. In general, TMA−ALD processing of thin alumina films on initially preoxidized copper substrates using O_2 half-cycles instead of H_2O offers a route to well-defined, carbon depleted, and dehydroxylated films. The high growth rate of ca. 3−4 Å/cycle was observed for TMA+O_2 ALD (O_2 half-cycles at 623 K, the surface with low carbon content).

ASSOCIATED CONTENT

Supporting Information

Cu $2p_{3/2}$ core level region for first 4 half-cycles, HREELS spectrum of Cu_2O/Cu(111) surface, pixel height histogram for STM images after first TMA cycle on Cu_2O/Cu(111), and explanation of image processing used in Figure 6. The Supporting Information is available free of charge on the ACS Publications website at DOI: 10.1021/acsami.5b03598.

AUTHOR INFORMATION

Corresponding Author

*D. Y. Zemlyanov. E-mail: dzemlian@purdue.edu.

Present Addresses

Amir Gharachorlou. Surface Characterization Lab, 3M Corporate Research Analytical Laboratory, 3M Center, Bldg. 201-S-272C, St. Paul, MN 55144-1000, United States

Michael D. Detwiler. BASF Corporation, 25 Middlesex/Essex Turnpike, Iselin, NJ 08830-0770, United States

Xiang-Kui Gu. Department of Chemical Engineering and Materials Science, Wayne State University, Detroit, Michigan 48202, United States

Author Contributions

⊥These authors contributed equally.

The paper was written through contributions of all authors. All authors have given approval to the final version of the paper.

Notes

The authors declare no competing financial interest.

ACKNOWLEDGMENTS

This material is based upon work supported as part of the Institute for Atom-efficient Chemical Transformations (IACT), an Energy Frontier Research Center funded by the U.S. Department of Energy, Office of Science, Office of Basic Energy Sciences. L. Mayr acknowledges financial support via FWF SFB "FOXSI" project part F4503-N16 and via a scholarship of the Carinthian Confederation of Industry (Industriellenvereinigung Kärnten). The authors acknowledge the Helmholtz-Zentrum Berlin for provision of synchrotron radiation beamtime at beamline ISISS-PGM of BESSY II (project 2013_1_121219) and thank the HZB/BESSY II staff members Michael Hävecker, Axel Knop-Gericke, and Mark Greiner for their support of the *in situ* XPS measurements at beamline ISISS-PGM.

ABBREVIATIONS

ALD, atomic layer deposition
HREELS, high-resolution electron energy loss spectroscopy
STM, scanning tunneling microscopy
TMA, trimethylaluminum
XPS, X-ray photoelectron spectroscopy

REFERENCES

(1) Abdulagatov, A. I.; Yan, Y.; Cooper, J. R.; Zhang, Y.; Gibbs, Z. M.; Cavanagh, A. S.; Yang, R. G.; Lee, Y. C.; George, S. M. Al_2O_3 and TiO_2 Atomic Layer Deposition on Copper for Water Corrosion Resistance. *ACS Appl. Mater. Interfaces* **2011**, *3* (12), 4593−4601.

(2) Kelly, J.; Parks, C.; Demarest, J.; Li, J.; Penny, C. Microstructure Evolution of Copper in Nanoscale Interconnect Features. In *Copper Electrodeposition for Nanofabrication of Electronics Devices*; Kondo, K.,

DOI: 10.1021/acsami.5b03598
ACS Appl. Mater. Interfaces 2015, 7, 16428−16439

Akolkar, R. N., Barkey, D. P., Yokoi, M., Eds.; Springer: New York, 2014; Chapter 6, pp 115−130.
(3) Ma, Y.; Evans, D. R.; Nguyen, T.; Ono, Y.; Hsu, S. T. Fabrication and Characterization of Sub-quarter-micron MOSFETs with a Copper Gate Electrode. *IEEE Electron Device Lett.* **1999**, *20* (5), 254−255.
(4) Gokhale, A. A.; Dumesic, J. A.; Mavrikakis, M. On the Mechanism of Low-Temperature Water Gas Shift Reaction on Copper. *J. Am. Chem. Soc.* **2008**, *130* (4), 1402−1414.
(5) Gu, X.-K.; Li, W.-X. First-Principles Study on the Origin of the Different Selectivities for Methanol Steam Reforming on Cu(111) and Pd(111). *J. Phys. Chem. C* **2010**, *114* (49), 21539−21547.
(6) O'Neill, B. J.; Jackson, D. H. K.; Crisci, A. J.; Farberow, C. A.; Shi, F.; Alba-Rubio, A. C.; Lu, J.; Dietrich, P. J.; Gu, X.; Marshall, C. L.; Stair, P. C.; Elam, J. W.; Miller, J. T.; Ribeiro, F. H.; Voyles, P. M.; Greeley, J.; Mavrikakis, M.; Scott, S. L.; Kuech, T. F.; Dumesic, J. A. Stabilization of Copper Catalysts for Liquid-Phase Reactions by Atomic Layer Deposition. *Angew. Chem., Int. Ed.* **2013**, *52* (51), 13808−13812.
(7) Chang, M. L.; Cheng, T. C.; Lin, M. C.; Lin, H. C.; Chen, M. J. Improvement of Oxidation Resistance of Copper by Atomic Layer Deposition. *Appl. Surf. Sci.* **2012**, *258* (24), 10128−10134.
(8) Riha, S. C.; Jin, S.; Baryshev, S. V.; Thimsen, E.; Wiederrecht, G. P.; Martinson, A. B. F. Stabilizing Cu2S for Photovoltaics One Atomic Layer at a Time. *ACS Appl. Mater. Interfaces* **2013**, *5* (20), 10302−10309.
(9) Alba-Rubio, A. C.; O'Neill, B. J.; Shi, F.; Akatay, C.; Canlas, C.; Li, T.; Winans, R.; Elam, J. W.; Stach, E. A.; Voyles, P. M.; Dumesic, J. A. Pore Structure and Bifunctional Catalyst Activity of Overlayers Applied by Atomic Layer Deposition on Copper Nanoparticles. *ACS Catal.* **2014**, *4*, 1554−1557.
(10) Zhang, H.; Gu, X.-K.; Canlas, C.; Kropf, A. J.; Aich, P.; Greeley, J. P.; Elam, J. W.; Meyers, R. J.; Dumesic, J. A.; Stair, P. C.; Marshall, C. L. Atomic Layer Deposition Overcoating: Tuning Catalyst Selectivity for Biomass Conversion. *Angew. Chem., Int. Ed.* **2014**, *53* (45), 12132−12136.
(11) Leskelä, M.; Ritala, M. Atomic Layer Deposition (ALD): From Precursors to Thin Film Structures. *Thin Solid Films* **2002**, *409* (1), 138−146.
(12) Puurunen, R. L. Surface Chemistry of Atomic Layer Deposition: A Case Study for the Trimethylaluminum/Water Process. *J. Appl. Phys.* **2005**, *97* (12), 121301−121352.
(13) Matsumoto, T.; Bennett, R. A.; Stone, P.; Yamada, T.; Domen, K.; Bowker, M. Scanning Tunneling Microscopy Studies of Oxygen Adsorption on Cu(111). *Surf. Sci.* **2001**, *471* (1−3), 225−245.
(14) Elliott, S. D.; Greer, J. C. Simulating the Atomic Layer Deposition of Alumina from First Principles. *J. Mater. Chem.* **2004**, *14* (21), 3246−3250.
(15) Hinch, B. J.; Dubois, L. H. Stable and Metastable Phases of Water Adsorbed on Cu(111). *J. Chem. Phys.* **1992**, *96* (4), 3262−3268.
(16) Yamamoto, S.; Andersson, K.; Bluhm, H.; Ketteler, G.; Starr, D. E.; Schiros, T.; Ogasawara, H.; Pettersson, L. G. M.; Salmeron, M.; Nilsson, A. Hydroxyl-induced wetting of metals by water at near-ambient conditions. *J. Phys. Chem. C* **2007**, *111* (22), 7848−7850.
(17) Lu, J. L.; Liu, B.; Guisinger, N. P.; Stair, P. C.; Greeley, J. P.; Elam, J. W. First-Principles Predictions and in Situ Experimental Validation of Alumina Atomic Layer Deposition on Metal Surfaces. *Chem. Mater.* **2014**, *26* (23), 6752−6761.
(18) Dillon, A. C.; Ott, A. W.; Way, J. D.; George, S. M. Surface-Chemistry of Al_2O_3 Deposition Using $Al(CH_3)_3$ and H_2O in a Binary Reaction Sequence. *Surf. Sci.* **1995**, *322* (1−3), 230−242.
(19) Puurunen, R. L.; Lindblad, M.; Root, A.; Krause, A. O. I. Successive reactions of gaseous trimethylaluminium and ammonia on porous alumina. *Phys. Chem. Chem. Phys.* **2001**, *3* (6), 1093−1102.
(20) Miikkulainen, V.; Leskela, M.; Ritala, M.; Puurunen, R. L. Crystallinity of Inorganic Films Grown by Atomic Layer Deposition: Overview and General Trends. *J. Appl. Phys.* **2013**, *113* (2), 021301.
(21) Elliott, S. D.; Scarel, G.; Wiemer, C.; Fanciulli, M.; Pavia, G. Ozone-Based Atomic Layer Deposition of Alumina from TMA: Growth, Morphology, and Reaction Mechanism. *Chem. Mater.* **2006**, *18* (16), 3764−3773.
(22) Kwon, J.; Dai, M.; Halls, M. D.; Chabal, Y. J. Detection of a Formate Surface Intermediate in the Atomic Layer Deposition of High-κ Dielectrics Using Ozone. *Chem. Mater.* **2008**, *20* (10), 3248−3250.
(23) Kwon, J.; Dai, M.; Halls, M. D.; Chabal, Y. J. Suppression of Substrate Oxidation During Ozone Based Atomic Layer Deposition of Al_2O_3: Effect of Ozone Flow Rate. *Appl. Phys. Lett.* **2010**, *97* (16), 162903−162905.
(24) Rai, V. R.; Vandalon, V.; Agarwal, S. Surface Reaction Mechanisms during Ozone and Oxygen Plasma Assisted Atomic Layer Deposition of Aluminum Oxide. *Langmuir* **2010**, *26* (17), 13732−13735.
(25) Heil, S. B. S.; van Hemmen, J. L.; van de Sanden, M. C. M.; Kessels, W. M. M. Reaction Mechanisms during Plasma-Assisted Atomic Layer Deposition of Metal Oxides: A Case Study for Al_2O_3. *J. Appl. Phys.* **2008**, *103* (10), 103302−103315.
(26) Langereis, E.; Keijmel, J.; van de Sanden, M. C. M.; Kessels, W. M. M. Surface Chemistry of Plasma-Assisted Atomic Layer Deposition of Al_2O_3 Studied by Infrared Spectroscopy. *Appl. Phys. Lett.* **2008**, *92* (23), 231904−231906.
(27) Horcas, I.; Fernández, R.; Gómez-Rodríguez, J. M.; Colchero, J.; Gómez-Herrero, J.; Baro, A. M. WSXM: A Software for Scanning Probe Microscopy and a Tool for Nanotechnology. *Rev. Sci. Instrum.* **2007**, *78* (1), 013705−013712.
(28) Salmeron, M.; Schlögl, R. Ambient Pressure Photoelectron Spectroscopy: a New Tool for Surface Science and Nanotechnology. *Surf. Sci. Rep.* **2008**, *63* (4), 169−199.
(29) Detwiler, M. D.; Gharachorlou, A.; Mayr, L.; Gu, X. K.; Liu, B.; Greeley, J.; Delgass, W. N.; Ribeiro, F. H.; Zemlyanov, D. Y. Reaction of Trimethylaluminum with Water on Pt(111) and Pd(111) from 10^{-5} to 10^{-1} Millibar. *J. Phys. Chem. C* **2015**, *119* (5), 2399−2411.
(30) Fairley, N. *CasaXPS*, 2.3.16dev85; Casa Software Ltd.: Teignmouth, U. K., 2011.
(31) Fadley, C. S. Basic Concepts of X-ray Photoelectron Spectroscopy. In *Electron Spectroscopy: Theory, Techniques and Applications*; Brundle, C. R., Baker, A. D., Eds.; Academic Press: New York, 1978; Vol. *2*, pp 1−156.
(32) Scofield, J. H. Hartree-Slater Subshell Photoionization Cross-Sections at 1254 and 1487 eV. *J. Electron Spectrosc. Relat. Phenom.* **1976**, *8* (2), 129−137.
(33) Yeh, J. J.; Lindau, I. Atomic Subshell Photoionization Cross Sections and Asymmetry Parameters: $1 \leqslant Z \leqslant 103$. *At. Data Nucl. Data Tables* **1985**, *32* (1), 1−155.
(34) Powell, C. J.; Jablonski, A. *NIST Electron Effective-Attenuation-Length Database*, Version 1.3; National Institute of Standards and Technology: Gaithersburg, MD, 2011.
(35) Gharachorlou, A.; Detwiler, M. D.; Nartova, A. V.; Lei, Y.; Lu, J.; Elam, J. W.; Delgass, W. N.; Ribeiro, F. H.; Zemlyanov, D. Y. Palladium Nanoparticle Formation on TiO_2(110) by Thermal Decomposition of Palladium(II) Hexafluoroacetylacetonate. *ACS Appl. Mater. Interfaces* **2014**, *6* (16), 14702−11.
(36) Smith, K. C.; Saenz, D. A.; Zemlyanov, D.; Voevodin, A. A. *XPS Thickness Solver*, September 2014 ed.; nanoHUB.org: West Lafayette, IN, 2012; https://nanohub.org/resources/xpsts.
(37) Kresse, G.; Furthmüller, J. Efficiency of Ab-initio Total Energy Calculations for Metals and Semiconductors Using a Plane-Wave Basis Set. *Comput. Mater. Sci.* **1996**, *6* (1), 15−50.
(38) Blöchl, P. E. Projector Augmented-Wave Method. *Phys. Rev. B: Condens. Matter Mater. Phys.* **1994**, *50* (24), 17953−17979.
(39) Perdew, J. P.; Wang, Y. Accurate and Simple Analytic Representation of the Electron-Gas Correlation Energy. *Phys. Rev. B: Condens. Matter Mater. Phys.* **1992**, *45* (23), 13244−13249.
(40) Jensen, F.; Besenbacher, F.; Lægsgaard, E.; Stensgaard, I. Oxidation of Cu(111): Two New Oxygen Induced Reconstructions. *Surf. Sci.* **1991**, *259* (3), L774−L780.

DOI: 10.1021/acsami.5b03598
ACS Appl. Mater. Interfaces 2015, 7, 16428−16439

(41) Jensen, F.; Besenbacher, F.; Stensgaard, I. Two New Oxygen Induced Reconstructions on Cu(111). *Surf. Sci.* **1992**, *269−270* (0), 400−404.
(42) Gharachorlou, A.; Detwiler, M. D.; Mayr, L.; Gu, X.-K.; Greeley, J.; Reifenberger, R. G.; Delgass, W. N.; Ribeiro, F. H.; Zemlyanov, D. Y. The Surface Chemistry of Trimethylaluminium on Pd(111) and Pt(111). *J. Phys. Chem. C* **2015**, 150318155756000.
(43) Moulder, J. F.; Chastain, J.; King, R. C. *Handbook of X-ray Photoelectron Spectroscopy: a Reference Book of Standard Spectra for Identification and Interpretation of XPS Data*; Physical Electronics: Eden Prairie, MN, 1995.
(44) Gu, X. K.; Liu, B.; Greeley, J. First-Principles Study of Structure Sensitivity of Ethylene Glycol Conversion on Platinum. *ACS Catal.* **2015**, *5* (4), 2623−2631.
(45) Ghijsen, J.; Tjeng, L. H.; Vanelp, J.; Eskes, H.; Westerink, J.; Sawatzky, G. A.; Czyzyk, M. T. Electronic-Structure of Cu_2O and CuO. *Phys. Rev. B: Condens. Matter Mater. Phys.* **1988**, *38* (16), 11322−11330.
(46) Lee, M. B.; Lee, J. H.; Frederick, B. G.; Richardson, N. V. Surface Structure of Ultra-Thin $A1_2O_3$ Films on Metal Substrates. *Surf. Sci.* **2000**, *448* (2−3), L207−L212.
(47) Frank, M.; Wolter, K.; Magg, N.; Heemeier, M.; Kühnemuth, R.; Bäumer, M.; Freund, H.-J. Phonons of Clean and Metal-Modified Oxide Films: an Infrared and HREELS Study. *Surf. Sci.* **2001**, *492* (3), 270−284.
(48) Lin, J. L.; Bent, B. E. Iodomethane dissociation on Cu(111): Bonding and Chemistry of Adsorbed Methyl Groups. *J. Vac. Sci. Technol., A* **1992**, *10* (4), 2202−2209.
(49) Chao-Ming, C.; Bent, B. E. Methyl Radical Adsorption on Cu(111): Bonding, Reactivity, and the Effect of Coadsorbed Iodine. *Surf. Sci.* **1992**, *279* (1−2), 79−88.
(50) Hinkle, C. L.; Sonnet, A. M.; Vogel, E. M.; McDonnell, S.; Hughes, G. J.; Milojevic, M.; Lee, B.; Aguirre-Tostado, F. S.; Choi, K. J.; Kim, H. C.; Kim, J.; Wallace, R. M. GaAs Interfacial Self-Cleaning by Atomic Layer Deposition. *Appl. Phys. Lett.* **2008**, *92* (7), 071901−071903.
(51) Ishiguro, T.; Kitazawa, A.; Mizutani, N.; Kato, M. Single-Crystal Growth and Crystal-Structure Refinement of $CuAlO_2$. *J. Solid State Chem.* **1981**, *40* (2), 170−174.
(52) Mulligan, A.; Dhanak, V.; Kadodwala, M. A High-Resolution Photoemission Study of Nanoscale Aluminum Oxide Films on NiAl(110). *Langmuir* **2005**, *21* (18), 8312−8318.
(53) Kovács, K.; Perczel, I. V.; Josepovits, V. K.; Kiss, G.; Réti, F.; Deák, P. In Situ Surface Analytical Investigation of the Thermal Oxidation of Ti−Al Intermetallics up to 1000 °C. *Appl. Surf. Sci.* **2002**, *200* (1−4), 185−195.
(54) Bianconi, A.; Bachrach, R. Z.; Hagstrom, S. B. M.; Flodstrom, S. A. Al-Al_2O_3 Interface Study Using Surface Soft-X-Ray Absorption and Photoemission Spectroscopy. *Phys. Rev. B: Condens. Matter Mater. Phys.* **1979**, *19* (6), 2837−2843.
(55) Mcconville, C. F.; Seymour, D. L.; Woodruff, D. P.; Bao, S. Synchrotron Radiation Core Level Photoemission Investigation of the Initial-Stages of Oxidation of Al(111). *Surf. Sci.* **1987**, *188* (1−2), 1−14.
(56) Kloprogge, J. T.; Duong, L. V.; Wood, B. J.; Frost, R. L. XPS Study of the Major Minerals in Bauxite: Gibbsite, Bayerite and Pseudo-Boehmite. *J. Colloid Interface Sci.* **2006**, *296* (2), 572−576.
(57) Sherwood, P. M. A. Introduction to Studies of Aluminum and its Compounds by XPS. *Surf. Sci. Spectra* **1998**, *5* (1), 1−3.
(58) Alexander, M. R.; Thompson, G. E.; Beamson, G. Characterization of the Oxide/Hydroxide Surface of Aluminium Using X-ray Photoelectron Spectroscopy: a Procedure for Curve Fitting the O 1s Core Level. *Surf. Interface Anal.* **2000**, *29* (7), 468−477.
(59) Maurel, C.; Abel, M.; Koudia, M.; Bocquet, F.; Porte, L. Pit Formation and Segregation Effects during Cu Thin-Film Growth on Ag(111). *Surf. Sci.* **2005**, *596* (1−3), 45−52.
(60) Xu, Y.; Mavrikakis, M. Adsorption and Dissociation of O_2 on Cu(111). Thermochemistry, Reaction Barrier and the Effect of Strain. *Surf. Sci.* **2001**, *494* (2), 131−144.
(61) Choi, M.; Lyons, J. L.; Janotti, A.; Van de Walle, C. G. Impact of Carbon and Nitrogen Impurities in High-κ Dielectrics on Metal-Oxide-Semiconductor Devices. *Appl. Phys. Lett.* **2013**, *102* (14), 142902−142905.

DOI: 10.1021/acsami.5b03598
ACS Appl. Mater. Interfaces 2015, 7, 16428−16439